DOI: 10.1002/ejic.200500775

Electrochemical Detection of High Oxidation States of Chromium(IV and V) in Chromium-Doped Cassiterite and Tin-Sphene Ceramic Pigmenting Systems

Antonio Doménech,*[a] Francisco Jose Torres,[b] Esther Ruiz de Sola,[b] and Javier Alarcón[b]

Keywords: Chromium / High oxidation states / Voltammetry / Cassiterite / Tin-sphene

Solid-state electrochemistry is applied to detect the presence of chromium centres with high oxidation states in chromium-doped cassiterite and tin-sphene ceramic pigmenting systems. Voltammetric data indicate that Cr^{V} and Cr^{IV} centres with different coordinative arrangements exist in the studied materials, and yield proton-assisted reduction processes at +0.95, +0.42 AgCl/Ag in contact with 0.50 M H_2SO_4. Electrochemical measurements are correlated with spectroscopic data. The Cr^{IV} and Cr^{V} metal ions display a significant light-driven electrocatalytic effect on the oxidation of 1,4-dihydrobenzoquinone and $Fe(CN)_6^{4-}$ ions that involves the formation of surface-confined adducts.

Introduction

Ceramic pigments are formed by crystalline phases containing cromophore cations. These materials are dispersed in particulate form in the bulk ceramic body or in the outer glassy layer on the ceramic support. During the thermal processing of ceramic materials, these particulate components must be stable at the high temperatures reached and must be inert to the chemical action of other components of the ceramic body, i.e. other crystalline phases and/or glassy phases.

Purple and pink chromium-containing, tin-based ceramic pigments have been widely used in the industry for years. Two of the main crystalline structures included in this group of ceramic pigments are cassiterite (SnO_2) and sphene or malayaite ($CaSnSiO_5$), which produce the purple and pink colours, respectively. As is well known, cassiterite has a rutile-type structure, while sphene possesses a titanite-type structure.

The preparation and characterisation of these two types of chromium-containing pigments have been widely studied by different authors for the past decades.[1,2] Different preparation procedures have been used in order to facilitate the kinetics of the reaction, which lead to the Cr-doped cassiterite or sphene particulate materials.[3–5] Microstructural features such as morphology, shape and size of the crystals, as well as important characteristics of particulate materials, have also been investigated extensively.[6,7]

The crystallochemistry of cassiterite and sphene structures indicates that the chromium cations in both structures are in octahedral sites, replacing the Sn^{IV} centres. There is agreement amongst various authors on this point. However, the controversy on the chemical states of the doped chromium cation exists for some time now.[6–11] Thus, Ren et al.,[8] on the basis of electron spin resonance spectroscopy, reflectance spectroscopy and magnetic susceptibility measurements, claimed that the violet colour of the Cr-SnO_2 pigment is caused by the simultaneous presence of Cr^{IV} and Cr^{III} ions, the former as a Cr^{IV}-SnO_2 solid solution and the latter as Cr_2O_3. López-Navarrete et al.[6–8] reached the same conclusion from X-ray photoelectron, diffuse reflectance and magnetic susceptibility data. More recently, these authors concluded that in Cr-doped sphene structures most of the tetravalent chromium cations form a solid solution with the sphene lattice by mostly substituting the Sn^{IV} cations in the isolated octahedral positions, while a very small amount of Cr^{IV} also substitutes the tetrahedral Si^{IV} ions. In contrast, Pavlov et al.,[10] from electronic absorption spectroscopy studies, concluded that the chromium cation is in the oxidation state +3 in Cr-SnO_2, while in the Cr-doped sphene there is an additional band in the near-IR part of the spectrum (around 1200 nm), which can be attributed to Cr^{IV}.

Recently, Julián et al.,[11] using a wet synthetic route, indicated that the violet colour in the Cr-SnO_2 pigmenting system is mainly produced by Cr^{III} and/or Cr^{IV} ions incorporated in the cassiterite structure. On the basis of electron spin resonance spectroscopy data, these authors concluded that different amounts of Cr^{V}, Cr^{IV} and Cr^{III} ions are present in chromium-doped cassiterite.

From the above reports it seems possible that in both ceramic-pigmenting systems, the chromium cation can be present in several oxidation states. However, it can also be

[a] Departament de Química Analítica, Universitat de València, Dr. Moliner, 50, 46100 Burjassot (València), Spain
E-mail: antonio.domenech@uv.es
[b] Departament de Química Inorgànica. Universitat de València, Dr. Moliner, 50, 46100 Burjassot (València) Spain
Supporting information for this article is available on the WWW under http://www.eurjic.org or from the author.

concluded that it is quite difficult to establish unambiguously the presence of these oxidation states of chromium in both host lattices from spectroscopic and magnetic techniques. Furthermore, the small amount of chromium in such materials makes it even more difficult to check the presence of Cr^{IV} or even Cr^{V} cations. Therefore, it would be interesting to use an experimental technique with enough sensitivity to distinguish between the different oxidation states of chromium in the Cr-doped cassiterite and Cr-doped sphene ceramic pigments. The coexistence of metal ions in different oxidation states is of interest in a wide variety of contexts. In particular, the simultaneous presence of Cr^{III} and Cr^{IV} in porous chromium-containing α-tin phosphate[12] and silica optical fibres[13] has been reported recently.

Over the last years the voltammetry of microparticles has emerged as a powerful technique to obtain chemical information on doped materials. Therefore, in this paper the possible presence of high oxidation states of chromium in the studied materials will be investigated by square wave voltammetry upon attachment of solid samples to paraffin-impregnated graphite electrodes (PIGEs). This follows the methodology of the voltammetry of microparticles approach, an increasingly growing research field for which extensive reviews are available.[14,15] The voltammetry of tin oxide microparticles and related compounds has not been described in detail in spite of the wide range of applications of tin oxide electrodes.[16] Recently, Scholz et al. described the electrochemistry of natural and synthetic tin sulfosalts using the voltammetry of microparticles methodology.[17] This scheme has previously been applied for studying the electrochemistry of SnO_2 and Sn-rich glazed ceramics.[18] Studies on nanosized SnO_2 particles dispersed on graphite electrodes,[19] nanocrystalline tin oxide electrodes[20] and modification of the film of SnO_2 nanocrystallites with organic reagents,[21] all devoted to the detection of selected analytes, have also been reported. The electrochemical dissolution of chromium oxides, spinels, and chromites has been studied by Blesa et al.[22–24] and Grygar et al.[25–27] Other reports on the solid-state electrochemistry of chromium concern chromium(II), hexacyanochromate(III),[28] some organic Cr complexes[29] and chromium oxide films deposited on stainless steel.[30] However, no detailed studies on the presence of high oxidation states of chromium have been reported.

The electrochemical reduction of chromate and dichromate in solution is complicated by adsorption processes.[31] Three reduction waves appear at acidic pH values for the electrochemical pathway involving any Cr^{IV} intermediate species.[32] However, intermediate Cr^{V} species have been electrochemically characterised in the oxidation of oxalic acid by chromic acid at pH 1.[33]

We report here on a solid-state electrochemical study devoted to the determination of the possible presence of high oxidation states of chromium in chromium-doped cassiterite and chromium-doped tin-sphene. For this purpose, solid samples were attached to paraffin-impregnated graphite electrodes in contact with electrolytic solutions of aqueous H_2SO_4 or $HClO_4$, and $NaClO_4$. Cyclic and square wave voltammetry were used as detection modes. The latter technique is of particular interest because of its high sensitivity and immunity to capacitive effects.[34] In an attempt to correlate voltammetric and spectroscopic data, the electrocatalytic effect of chromium-doped materials on the oxidation of hexacyanoferrate(II) ions and 1,4-dihydrobenzoquinone in aqueous solution has been studied. Apart from its applications in chemical sensing and electrosynthesis, such catalytic processes can be used as amplifiers of the electrochemical properties of the catalytic centres, as illustrated by prior data on vanadium-doped zirconias and cobalt-containing cordierite materials.[35–37]

Results and Discussion

Characterisation of Chromium-containing Cassiterite and Sphene

X-ray diffraction patterns of the ceramic pigmenting systems, based on cassiterite and sphene structures, are supplied in the Supporting Information. The formation of a crystalline phase with a sphene structure is displayed in samples M-1 to M-4, after thermal treatment at 1300 °C and a 2-h holding time. In accordance with the JCPD card number 70-0437, all peaks can be associated with the main crystalline phase. It is worth noting that a small amount of SnO_2 is still present in the sample of M-2. For samples M-5 and M-6, the only crystalline phase detected is that of the cassiterite structure (JCPD card number 41-1445).

The diffuse reflectance spectra of both types of samples, i.e. cassiterite- and sphene-based structures, are shown in Figure 1. For the Cr-sphene specimens, two bands around 540 nm and 1200 nm are detected. The first one is attributed to the $^4A_{2g}$–$^4T_{2g}$ spin-allowed transition of the Cr^{III} ion with octahedral coordination,[10] as well as to the Cr^{IV} centres.[9,38] The band in the near-infrared part of the spectrum, centred at 1200 nm, is assigned to $^3A_2$–$^3T_1$ transitions of Cr^{IV} in tetrahedral surroundings.[9,39] The sphene structure can be described as composed of chains of corner-sharing SnO_6 octahedra running parallel to the cell edges that are cross-linked by silicate tetrahedra to form a $SnOSiO_4$ framework that accommodates Ca^{2+} in irregular hepta-coordinated polyhedra. Here, López-Navarrete et al.[9] recently suggested that Cr^{IV} replaced the partially octahedral Sn^{IV} and tetrahedral Si^{IV} sites.

The spectra of the chromium-containing cassiterite consist of a strong band at 560 nm and a weak band at 740 nm, which are attributed to Cr^{III} with octahedral coordination. However, the first band has also been ascribed to Cr^{IV} ions with octahedral symmetry.[9] In contrast to the Cr-sphene-based materials, in the cassiterite-derived materials there is no band around 1200 nm. The reason for the absence of the band associated with the Cr^{IV} ions with tetrahedral coordination is that there are no available tetrahedral sites in this structure.

The investigation by FESEM of the final ceramic pigments indicates that the particles that have formed have a

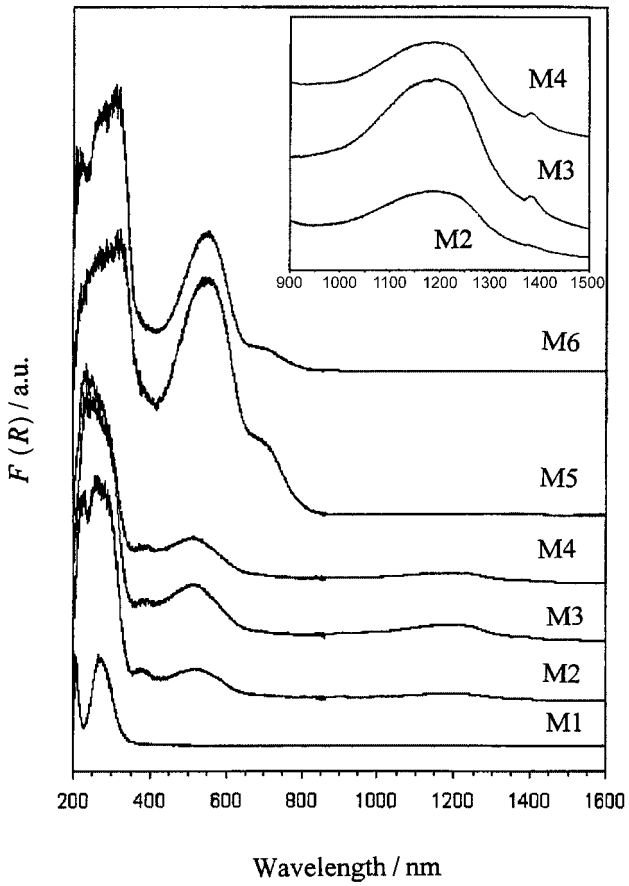

Figure 1. UV/Vis spectra of specimens thermally treated at final temperatures for 2 h: M-1 at 1400 °C and M-5 and M-6 at 1300 °C.

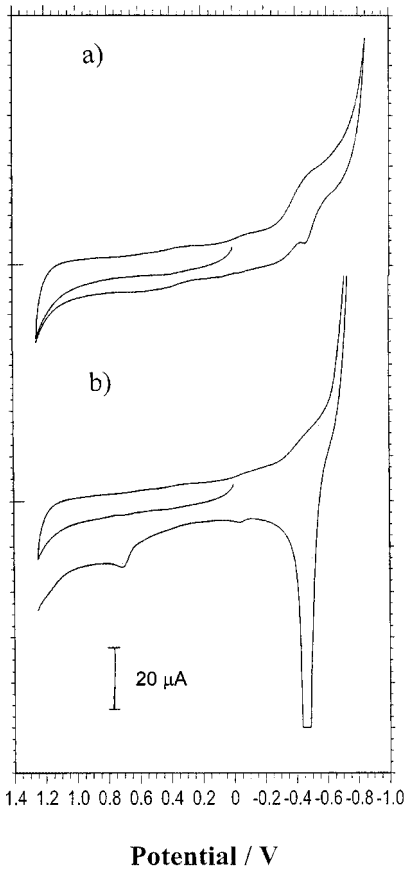

Figure 2. CVs of PIGEs modified by: (a) M-2, and (b) M-5, immersed in 0.50 M H_2SO_4. Potential scan rate 50 mV s^{-1}.

well-defined morphology. Micrographs of samples of M-4 and M-6 are shown in the Supporting Information. The discrete particles are prismatic and their sizes are smaller than 2 μm long and 0.5 μm wide.

Electrochemical Study of Prepared Materials

The electrochemistry of the studied materials is, in principle, dominated by tin-centred processes. This can be seen in Figure 2, in which the cyclic voltammograms (CVs) of: (a) M-2 and (b) M-5 in 0.50 M H_2SO_4 are shown. Such voltammograms are essentially identical to those recorded for sphene and cassiterite, respectively. For M-2 a reduction peak at –0.55 V vs. AgCl/Ag appears, followed by a prominent reduction current increasing from –0.70 V. In the reverse scan, a weak anodic peak near –0.50 V appears. The response of M-5 was similar, but here a prominent cathodic current appears at –0.55 V, while in the subsequent anodic scan a well-defined tall peak at –0.50 V is recorded. This corresponds, as described in detail elsewhere,[18] to the stripping oxidation of Sn to Sn^{2+} in solution, thus denoting that the prior cathodic step results in the formation of a deposit of Sn metal. In the positive region of potentials, a weak anodic peak near +0.5 V is also recorded.

Sn-centred electrochemical processes can be described in terms of the reduction of Sn^{IV} via the stepwise formation of solid Sn^{II} to Sn metal. These electrochemical processes can be represented for cassiterite as:

$$SnO_2(s) + 2\ H^+ + 2e^- \rightarrow x\ SnO(s) + (1 - x)\ Sn^{2+}(aq) + H_2O \quad (1)$$

$$SnO(s) + 2\ H^+ + 2e^- \rightarrow Sn(s) + H_2O \quad (2)$$

$$Sn^{2+}(aq) + 2\ e^- \rightarrow Sn(s) \quad (3)$$

(s) denotes the solid phases.

On scanning the potential in the positive direction, after a reductive step, the metal deposits generated electrochemically are oxidized to Sn^{2+} ions and SnO^{2+} in the solution phase:

$$Sn(s) \rightarrow Sn^{2+}(aq) + 2\ e^- \quad (4)$$

$$Sn^{2+}(aq) + H_2O \rightarrow SnO^{2+}(aq) + 2\ H^+ + 2\ e^- \quad (5)$$

this last step is responsible for the oxidation signal at +0.5 V.

Chromium-centred processes were studied for sample-modified PIGEs upon immersion into an electrolytic solution of H_2SO_4 or $HClO_4$, and $NaClO_4$. To prevent the appearance of tin-centred electrochemical processes, potentials between 0.0 and +1450 mV were routinely used. The response of Cr_2O_3, taken as a reference in this potential

range, is illustrated by the square wave voltammograms (SQWVs) in Figure 3. On scanning the potential in the positive direction, a prominent oxidation wave (I) is recorded at +1340 mV (Figure 3, a). This peak shows well-defined anodic and cathodic components of the square wave current, thus suggesting a quasi-reversible behaviour.[34] Following Grygar et al.,[25–27] this wave corresponds to the oxidative dissolution process:

$$Cr_2O_3(s) + 4\ H_2O \rightarrow Cr_2O_7^{2-} + 8\ H^+ + 6\ e^- \quad (6)$$

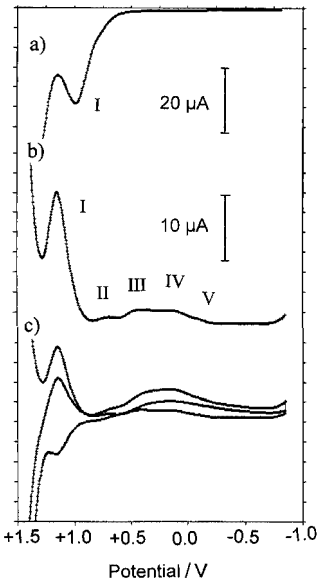

Figure 3. SQWV of Cr_2O_3 in contact with 0.10 M $HClO_4$ and 0.15 M $NaClO_4$. (a) potential scan initiated at –0.25 V in the positive direction; (b) potential scan initiated at +1.45 V in the negative direction; (c) id. with separate plots for the forward, backward and current increment vs. potential. Potential step increment 4 mV; square wave amplitude 25 mV; frequency 15 Hz.

On scanning the potential from +1450 mV in the negative direction, a peak near +1240 mV appears (I), followed by overlapping peaks at +700, +430, +250 and 0 mV (labelled as II, III, IV and V, respectively), as depicted in Figure 3 (b). The peak at +1240 mV corresponds to the oxidation of Cr_2O_3, as represented by Equation (6), and also appears when the potential is scanned in the positive direction because square wave voltammetry provides simultaneous inspection of both oxidation and reduction processes. Peaks II–V decrease rapidly until they disappear altogether when the potential scan is initiated at potentials below +950 mV, a potential for which no significant oxidative dissolution of Cr_2O_3 takes place; thus this denotes that such electrochemical processes are due to chromium species in solution generated during the electrochemical oxidation of chromium oxide.

The peak potential of I shifts positively on increasing the square wave frequency, *f*, while peaks II, III and IV remain essentially independent of *f* in the frequency range between 5 and 200 Hz [E_p(I) = +1140 ± 20 + (68 ± 2)log *f* (*N* = 9, *r* = 0.994)]. In this frequency range, peak V shifts to negative potentials on increasing the square wave frequency [E_p(V) = +145 ± 5 – (65 ± 5)log *f* (*N* = 9, *r* = 0.991)]. Interestingly, separate plots of the anodic and cathodic contributions to the square wave current, measured at the start and end of potential pulses, provided well-defined anodic and cathodic components for the peak at +1215 mV. However, peaks II–V exhibit only cathodic contributions as can be seen in Figure 3 (c): this denotes that these are essentially irreversible reduction processes.[34] These processes can be attributed to the stepwise reduction of $Cr_2O_7^{2-}$ ions in solution generated in the oxidative dissolution of Cr_2O_3. Electrochemical reduction of dichromate to Cr^{III} and Cr^{II} involves the formation of Cr^{V} and Cr^{IV} intermediates by processes II and III, but Cr^{IV} is thermodynamically unstable in solution and disproportionates into Cr^{III} and Cr^{VI}:[22]

$$6\ Cr^{IV} \rightarrow 4\ Cr^{3+} + Cr_2O_7^{2-} \quad (7)$$

Peak II is therefore enhanced with respect to peak III.

SQWVs of the studied materials exhibited some significant differences compared with those of Cr_2O_3. To clearly discriminate from the chromium-centred processes, in all cases, the SQWV of cassiterite and sphene was subtracted from that of the corresponding chromium-doped material. Thus, as shown in Figure 4 for: (a) M-2, and (b) M-5, the peak I appears at potentials that are more positive than that for Cr_2O_3 (+1290 mV) and is lowered. For samples M-2, M-3 and M-4 (Figure 4, a), an additional well-defined peak at +970 mV (VI) appears that precedes the separated peaks at +420 (VII), –30 (VIII) and –420 mV (IX). The peak VII exhibits a tall profile, suggesting that it corresponds to different electrochemical processes from those recorded for Cr_2O_3 at similar potentials. For samples M-5 and M-6 (see Figure 4, b), the peak VI is well developed and enhanced with respect to peaks VII, VIII and IX. Remarkably, peaks VI, VII, VIII and IX are enhanced on decreasing the frequency, a property typical of electrochemical processes involving solid phases.

Peaks VIII and IX shift to negative potentials on increasing the frequency [E_p(VIII) = 40 ± 5 – (60 ± 3)log *f* (*N* = 7, *r* = 0.997); E_p(IX) = –275 ± 5 – (99 ± 6)log *f* (*N* = 9, *r* = 0.992)], while peaks VI and VII remain essentially independent of frequency. On initiating the potential scan at +1050 mV, i.e. at a potential at which no significant oxidative dissolution of chromium centres occurs, peaks VI–IX appear with no significant decrease when compared with voltammograms initiated at +1450 mV. The above features are in contrast with those of the SQWV of Cr_2O_3 – peaks III–V decrease significantly on lowering the starting potential below +1250 mV.

The differences between Cr_2O_3 and the studied materials can be seen in Figure 5 in which the charge passed through processes III and VII (q_{III}, q_{VII}), calculated as the area under the voltammetric peak, is plotted as a function of the starting potential of the SQWVs, E_i. For chromium oxide, a fast decrease of q_{III} with decreasing E_i is obtained, whereas for the studied materials q_{III} becomes insensitive to changes in E_i at starting potentials below +950 mV.

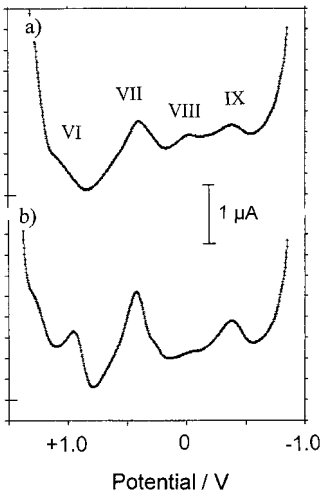

Figure 4. Semi-derivative convolution of SQWVs of : (a) M-2, and (b) M-5 immersed into 0.10 M $HClO_4$ and 0.15 M $NaClO_4$ after subtracting the SQWV of sphene and cassiterite, respectively. Potential scan initiated at +1.45 V in the negative direction. Potential step increment 4 mV; square wave amplitude 25 mV; frequency 5 Hz.

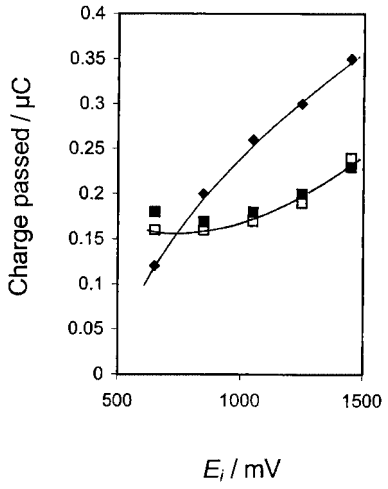

Figure 5. Variation of the charge passed during the electrochemical process III/VII with the starting potential of the SQWVs for diamonds: Cr_2O_3; squares: M-3; solid squares: M-6. Electrolyte: 0.10 M $HClO_4$ and 0.15 M $NaClO_4$. Potential step increment 4 mV; square wave amplitude 25 mV; frequency 5 Hz.

In the pH range between 1.5 and 4.0, peaks VII and IX shift to negative potentials on increasing the pH. For M-5, SQWVs with a potential step increment of 4 mV, a square wave amplitude of 25 mV and a frequency of 15 Hz produced: E_p(VII) = 585 ± 5 – (97 ± 6)pH (N = 7; r = 0.993); E_p(IX) = –255 ± 5 – (78 ± 6)pH (N = 7, r = 0.992). Peaks VI and VIII are essentially pH independent.

The voltammetric profile of peaks VI and VII is significantly different from that of peaks II–V recorded for Cr_2O_3. Remarkably, the peaks VI and VII exhibit well-developed anodic and cathodic components of the square wave current, as can be seen in Figure 6 for M-5. Here, peaks VIII and IX behave irreversibly.

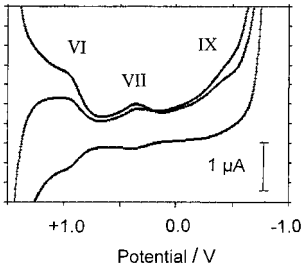

Figure 6. Separate forward, backward and current increment vs. potential graphs for the SQWVs of M-3 immersed in 0.10 M $HClO_4$ and 0.15 M $NaClO_4$. Potential scan initiated at +1.45 V in the negative direction. Potential step increment 4 mV; square wave amplitude 25 mV; frequency 15 Hz.

On comparing the SQWVs in Figure 6 with those depicted in Figure 3 (c), corresponding to Cr_2O_3, one can appreciate a notable increase in the reversibility of the electrochemical processes of VI and VII of the studied materials in contrast with the processes II–IV recorded for chromium oxide.

Additionally, peak VII is significantly enhanced in chromium-doped materials relative to peak I, while peaks II and IV disappear. Since it is not possible to control the exact amount of material transferred to the electrode, the quotients between the peak currents were used for comparing the voltammetric response of the studied materials with that of Cr_2O_3. Thus, the quotient between the peak currents of VII and I for chromium-doped materials, i_p(VII)/i_p(I), is larger than the i_p(III)/i_p(I) ratio determined for chromium(III) oxide. Interestingly, the i_p(VII)/i_p(I) ratio for M-3 increases abruptly at low frequencies, as can be seen in Figure 5. This behaviour is in contrast with that observed for Cr_2O_3. Here, as shown in Figure 7, the i_p(III)/i_p(I) ratio increases slowly on decreasing the frequency. For all chromium-doped cassiterites and chromium-doped sphenes, the i_p(VII)/i_p(I) ratio increases on increasing the chromium content. Pertinent peak potential data are summarised in Table 1.

All these data suggest that an amount of high oxidation states of chromium exists in the studied materials. Accordingly, the response of such materials results from the superimposition of solution processes initiated in the oxidative dissolution of Cr^{III}, which is similar to those described for Cr_2O_3, and a solid-state pathway starting from the reduction of chromium centres that exist in high oxidation states of the solids. Then, peak VI can be attributed to the reduction of Cr^{V} centres mainly existing in chromium-doped cassiterite, while the peak VII, which prevails in chromium-doped sphenes, is attributable to the reduction of pristine Cr^{IV} centres. In view of the possible presence of Cr^{IV} centres in two different coordinations, peaks VII and VIII can be associated with the reduction of differently coordinated Cr^{IV} units. This assignment is consistent with prior data showing the existence of site-characteristic voltammetric responses in vanadium-doped zircon,[35] zirconia[36] and cobalt cordierites[37] and appears to be in agreement with spectral data (vide infra). In this scheme, pro-

Table 1. Peak potential and peak current data for Cr_2O_3 and chromium-doped materials from SQWVs recorded at sample-modified PIGEs in contact with H_2SO_4 and 0.15 M $NaClO_4$, pH = 1.7. Potential step increment 4 mV; square wave amplitude 25 mV; frequency 15 Hz.

Modifier	E_p (I) [mV]	E_p(VI) [mV]	E_p(II) [mV]	E_p(III) [mV]	E_p(VII) [mV]	E_p(IV) [mV]	i_p(VII)/i_p(I)	i_p(III)/i_p(I)	i_p(III′)/i_p(I)
Cr_2O_3	+1215	–	+700	+480	–	+230	–	0.39	–
M-2	+1300	+970	–	–	+420	–	0.25	–	0.44
M-3	+1305	+970	–	–	+410	–	0.64	–	0.56
M-4	+1305	+995	–	–	+405	–	0.26	–	0.48
M-5	+1320	+990	–	–	+420	–	0.22	–	0.40
M-6	+1305	+985	–	–	+400	–	0.23	–	0.42

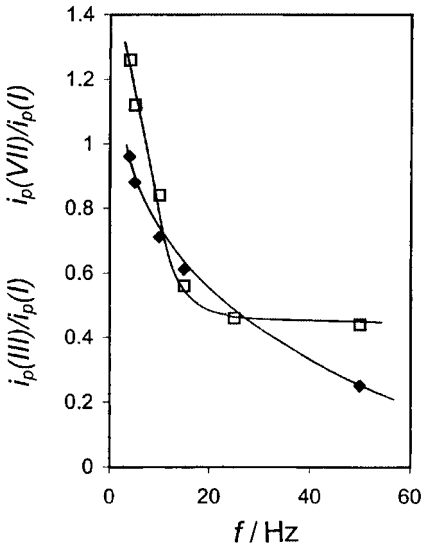

Figure 7. Variation with the square wave frequency of: i_p(VI)/i_p(I) ratio for M-6 (squares) and the i_p(III)/i_p(I) ratio for Cr_2O_3 (rhombs). (From SQWVs of sample-modified PIGEs immersed in 0.10 M $HClO_4$ and 0.15 M $NaClO_4$). Potential step increment 4 mV; square wave amplitude 25 mV.

cesses VI–VIII can be described in terms of solid-state redox reactions yielding Cr^{IV} and Cr^{III} centres. Under the experimental conditions employed here, both processes behave reversibly in such a way that proton transfer does not affect the overall reaction rate.

Electrochemical Pathway

This reaction scheme can, in principle, be related to the model of Lovric, Scholz, Oldham and co-workers for describing the electrochemistry of insulating solids.[40–43] Redox conductivity occurs by electron hopping between adjacent redox centres and by the exchange of ions or protons with the electrolyte, as a consequence of the gradient of the electrochemical potential in the particle.

In the studied cases, the propagation of the redox reaction through the solid microparticle requires the presence of appropriate redox-active centres on the surface of the particles and free access of protons or electrolyte ions from the supporting electrolyte. The foregoing considerations also apply for the fast charge transfer observed for organic complexes of Cr,[44] metallocenes[45] and organic compounds.[46]

Subsequent reduction of the Cr^{IV} centres to Cr^{III} centres involves two irreversible proton-assisted reduction processes that probably result in the formation of Cr^{III} centres in the solid phase (peak VII) and in solution through the processes VIII–IX.

It should be noted that in this solid-state pathway the Cr^{IV} oxidation state is stabilised with respect to disproportionation, as denoted by the appearance of the well-resolved, separated peak III′.

Following a scheme similar to that previously postulated for vanadium-doped zirconias,[37] formation of Cr^{V} centres may be described in terms of a process involving the insertion of OH groups and lattice distortion. Formally this can be represented as:

$$Sn_{1-x}Cr^{III}{}_xO_{2-x/2} + 2y\ OH^- \rightarrow Sn_{1-x}Cr^{III}{}_{x-y}Cr^{V}{}_yO_{2-x/2}(OH)_{2y} + 2y\ e^- \quad (8)$$

This picture is, in principle, consistent with the reaction schemes proposed for the oxidative dissolution of chromium oxides by oxometallates. According to Blesa et al., the reaction with oxometallates proceeds by oxygen transfer from the oxidant to surface Cr^{III} sites and is mediated by the oxo bridge Cr–O–M.[21–23] Then, peak VI at +970 mV can be attributed to the reduction of Cr^{V} surface centres to Cr^{IV} centres. To describe this kind of electrode process, it is assumed that a fraction of the total Cr^{V} centres is reduced to Cr^{IV} ones with concomitant loss of OH^- groups to ensure charge conservation and provide minor lattice distortion. Tentatively, this process can be represented by the redox reaction:

$$Sn_{1-x}Cr^{III}{}_{x-y}Cr^{V}{}_yO_{2-x/2}(OH)_{2y} + y\ e^- \rightarrow Sn_{1-x}Cr^{III}{}_{x-y}Cr^{IV}{}_yO_{2-x/2}(OH)_y + y\ OH^- \quad (9)$$

Cr^{IV} centres are subsequently reduced to Cr^{III} centres. Following the above criteria, this reduction process (peak VII at +420 mV) can be formulated for cassiterite as:

$$Sn_{1-x}Cr^{III}{}_{x-y}Cr^{IV}{}_yO_{2-x/2}(OH)_y + y\ e^- \rightarrow Sn_{1-x}Cr^{III}{}_{x-y}Cr^{IV}{}_yO_{2-x/2} + y\ OH^- \quad (10)$$

Reduction of the Cr^{IV} centres in sphene probably involves two different processes that correspond to the octahedral Cr^{IV} centres substituting for Sn^{IV} and tetrahedral Cr^{IV} centres substituting for Si^{IV}. Such electrode processes

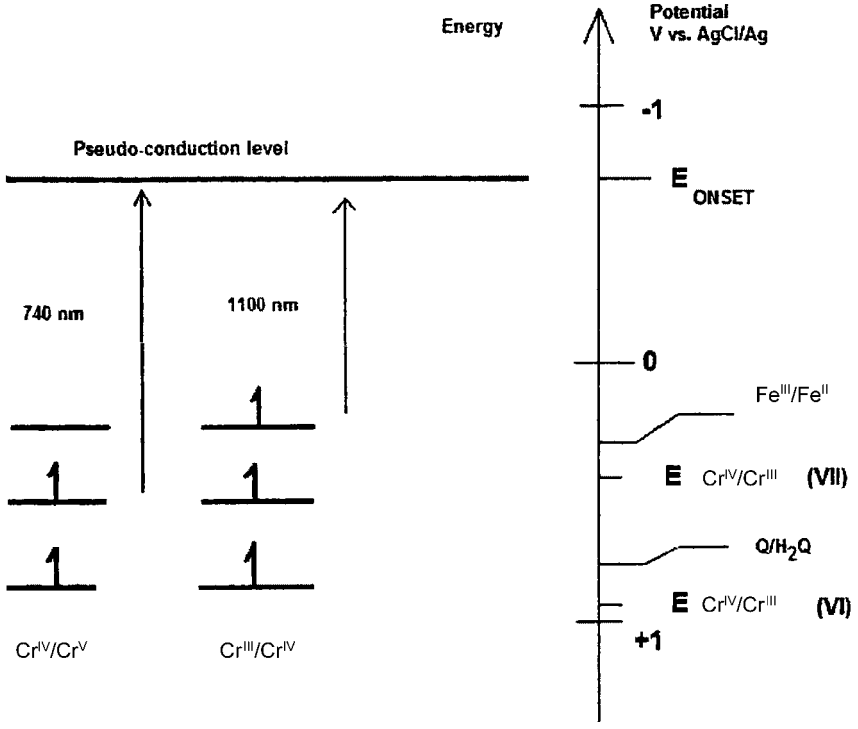

Figure 8. Energy/redox potential diagram for correlating spectrophotometric and electrochemical data in Cr-doped cassiterite and Cr-doped sphene.

can correspond to peak VIII and eventually can form Cr^{3+} ions in solution:

$$CaSn_{1-x}Cr^{III}_{x-y}Cr^{V}_{y}SiO_{5-x/2}(OH)_y + y\ H^+ + y\ e^- \rightarrow CaSn_{1-x}Cr^{III}_{x}SiO_{5-x/2} + y\ H_2O \quad (11)$$

Finally, the peak IX can be attributed to the reduction of Cr^{3+} to Cr^{2+} in the solution phase.

Correlation Between Spectral and Electrochemical Data

Correlation between electrochemical and spectroscopic data in solids usually focuses on the determination of the bandgap energy and the electrochemical HOMO and LUMO energies (E^{HOMO}, E^{LUMO}), corresponding to the estimated position of the upper edge of the valence band (HOMO) and the lower edge of the conduction band (LUMO).[47] In our case, spectral properties of chromium centres can be correlated with formal electrode potentials on the basis of energy diagrams of the 3d energy states of Cr^{III}, Cr^{IV}, and Cr^{V} proposed by Sakai et al.,[48] and Moretti and Michel-Calendini[49] with respect to the cluster valence edge of chromium-doped $BaTiO_3$ and to those recently calculated by Long et al.[50] for describing the spectra of Cr^{III}-doped $LaSc_3(BO_3)_4$, by Torchia et al.[51] for Cr^{III} ions in $LiNbO_3$, by Kammoun[52] for Cr^{IV} ions in $LiAlO_2$ and by Herren et al.[53] for Cr^{V} in chromium-doped SiO_2 glass.

From this one can attribute energies of 2.06, 0.98 and 0.36 eV to the Cr^{III} ($^4A_2$ state), Cr^{IV} ($^3T_1$) and Cr^{V} ($^2T_2$) centres in octahedral coordination, respectively, relative to the valence band edge corresponding to the O 2p t_{1g} level relevant to the MO_6 cluster. Term energies for crystal field transitions are: Cr^{III} ($^4A_2 \rightarrow {}^4T_1$, $^4T_2$) 2.10 eV; Cr^{IV} ($^3T_1 \rightarrow {}^1T_2$) 1.26 eV; Cr^{V} ($^2T_2 \rightarrow {}^2E_2$) 2.60 eV.[50–53] Formal electrode potentials are correlated with the vacuum level by assuming that the normal hydrogen electrode is 4.4 eV below the vacuum level.[54,55] Accordingly, the AgCl/Ag electrode will be 4.6 eV below the vacuum level. The corresponding energy diagram is shown in Figure 8. The upper edge of the valence band can in principle be approached by the voltammetric onset potential obtained from the intersection of the two tangents drawn at the rising current and the baseline charging current of the curves for the oxidation process.[56,57] The onset potential taken from the rising background current in Figure 4 was +1.43 V. Examination of the energy diagram in Figure 8 reveals that formal electrode potentials for the Cr^{V}/Cr^{IV} and Cr^{IV}/Cr^{III} couples are close to the vacuum energy levels for Cr^{V} and Cr^{IV} ions, respectively.

Electrocatalytic Processes

As already reported,[36,37] inorganic materials doped with electroactive species can exert a significant catalytic effect on selected electrochemical processes. Thus, Figure 9 shows a comparison of the CVs recorded in a 0.50 mM $K_4Fe(CN)_6$ and a 0.50 M H_2SO_4 solution at: (a) bare PIGE, (b) M-3 under dark conditions and (c) M-3 under Vis-IR illumination. As can be seen in Figure 9 (a), at the unmodified PIGE, the CVs of $Fe(CN)_6^{4-}$ solutions exhibit a well-defined reversible couple at peak potentials of +445 (anodic) and +335 mV (cathodic). For electrodes modified with chromium-doped materials under "dark" conditions, the

anodic portion of the CV becomes significantly modified. As can be seen in Figure 9 (b), an additional peak at +620 mV appears coupled with a weak cathodic signal near +580 mV and the overall peak current is enhanced. For samples M-2, M-3 and M-4, this response changes upon illumination. As can be seen in Figure 9 (c) for M-3, the current is depleted, while the peak at +620 mV vanishes. However, for samples M-5 and M-6 the catalytic effect remains insensitive to illumination with visible light.

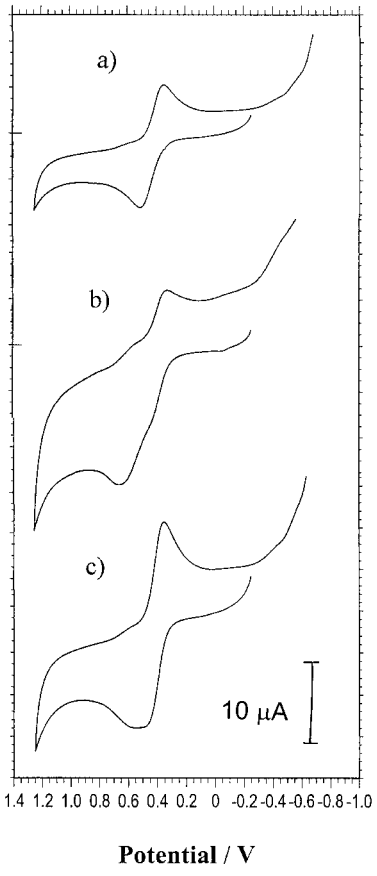

Figure 9. CVs recorded in a 0.50 mM $K_4Fe(CN)_6$ and 0.50 M H_2SO_4 solution at: a) bare PIGE; b) M-3-modified electrode under dark conditions, and c) M-3-modified electrode under illumination. Potential scan rate 50 mV s^{-1}.

The anodic peak at +620 mV can be attributed to the modifier-mediated oxidation of $Fe(CN)_6^{4-}$. In view of the close proximity of the potentials for the $Fe(CN)_6^{3-}/Fe(CN)_6^{4-}$, Cr^V/Cr^{IV} and Cr^{IV}/Cr^{III} couples, the catalytic effect can, in principle, be attributed to both Cr^V and Cr^{IV} centres, in agreement with the theory for mediated electrocatalysis.[58] The observed voltammetric profile can be interpreted in terms of the formation of a surface (chromium centre)–$Fe(CN)_6^{4-}$ adduct and the superimposition of the currents for the nonmediated (peak at +440 mV) and mediated (peak at +620 mV) oxidation of $Fe(CN)_6^{4-}$.

This is consistent with the variation with the frequency of the SQWVs illustrated in Figure 10 for M-4 in contact with 0.50 mM $K_4Fe(CN)_6$ and 0.50 M H_2SO_4. The peak at +620 mV is enhanced as the frequency decreases, in agreement with the assignment of this peak to the oxidation of a surface-confined species.

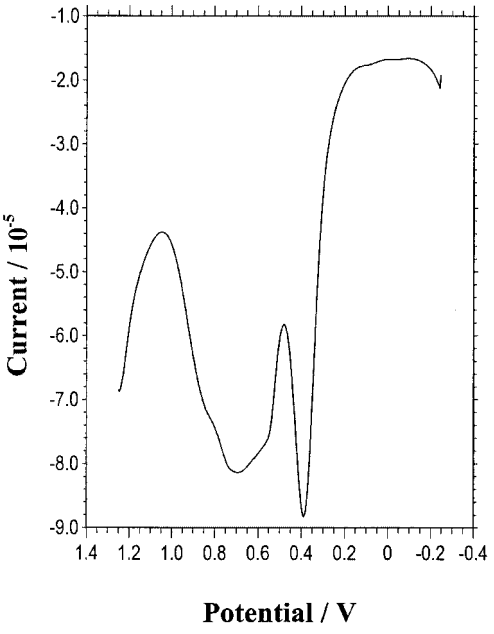

Figure 10. SQWV of a 0.50 mM $K_4Fe(CN)_6$ and 0.50 M H_2SO_4 solution at an M-4-modified electrode under dark conditions. Potential step increment 4 mV; square wave amplitude 25 mV; frequency 25 Hz.

The decrease in the catalytic ability of samples M-2, M-3 and M-4 under illumination can be rationalised on the basis of previously discussed spectroscopic data assuming that Cr^{IV} centres act as catalytic sites, as suggested by the close vicinity of its redox potential (+420 mV) and that of the $Fe(CN)_6^{3-}/Fe(CN)_6^{4-}$ couple (+390 mV). Upon illumination, there is excitation of Cr^{IV} centres that is equivalent, in agreement with literature data,[50,53] to a negative potential shift of 1.03 V of the Cr^{IV}/Cr^{III} couple, as schematised in Figure 8. These features result in a significant decrease in the catalytic ability of chromium centres, which is reflected in the lowering of the peak current.

Comparable features were obtained for the electrocatalyis of 1,4-dihydrobenzoquinone (H_2Q) oxidation, illustrated in Figure 11 for a 0.40 mM solution of H_2Q in 0.50 M H_2SO_4. As depicted in Figure 11 (a), at a bare graphite electrode, two overlapping anodic peaks appear at +700 and +850 mV, corresponding, in agreement with extensive literature on the electrochemistry of H_2Q, to the stepwise oxidation of hydroquinone to quinone:[59,60]

$$H_2Q \rightarrow Q + 2\,H^+ + 2\,e^- \quad (12)$$

As shown in Figure 11 (b) for M-6, the current for H_2Q oxidation is enhanced at electrodes modified with Cr-doped cassiterite under dark conditions. Again, the catalytic effect decreases upon illumination with visible light, as can be seen in Figure 11 (c). Remarkably, the catalytic effect is almost entirely absent for Cr-doped sphene samples. Such electrochemical data can again be interpreted with the help of the energy/redox potential diagram in Figure 8. Here, the

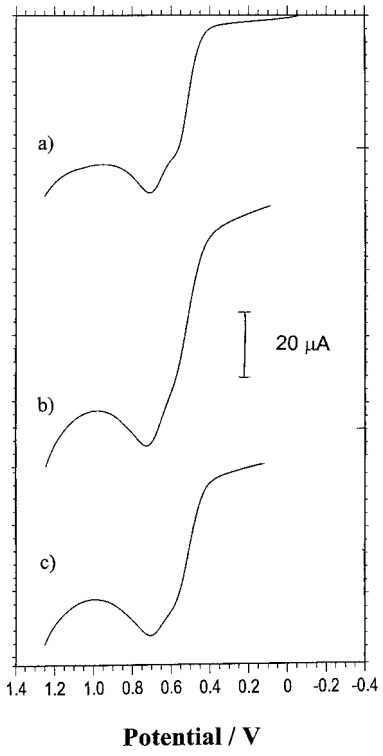

Figure 11. LSVs of a 0.40 mM solution of 1,4-dihydrobenzoquinone in 0.50 M H_2SO_4 at: a) bare PIGE; b) M-6 under dark conditions; and c) M-6 under illumination. Potential scan rate 20 mV s^{-1}.

formal potential of the Cr^V/Cr^{IV} couple (+970 mV) is close to the redox potential for H_2Q oxidation (+850 mV), thus suggesting that the Cr^V species in Cr-doped cassiterite are now catalytically active. Excitation of Cr^V centres upon illumination involves a gain in energy of 2.60 eV,[48,53] equivalent to a significant negative shift of the potential of the Cr^V/Cr^{IV}. Accordingly, illumination produces a significant decrease in the catalytic ability of Cr^V centres in chromium-doped cassiterite.

Final Considerations

Solid-state electrochemical data suggest that Cr^V and Cr^{IV} centres exist in chromium-doped cassiterite and sphene materials. The well-defined reduction of Cr^V centres to Cr^{IV} ones occurs at +0.97 mV for Cr-doped SnO_2. The oxidation state Cr^{IV} prevails in Cr-doped sphene, where the solid-state Cr^{IV} to Cr^{III} reduction takes place at +420 mV.

Cr^{IV} centres produce a significant catalytic effect on the electrochemical oxidation of $Fe(CN)_6^{4-}$ ions in acidic aqueous media. For chromium-doped sphenes the electrocatalytic effect decreases upon visible light irradiation. Electrochemical and spectroscopic data are consistent with an electrocatalytic pathway involving the formation of a surface-confined Cr^{IV}–hexacyanoferrate(II) adduct. Similarly, the oxidation of 1,4-dihydrobenzoquinone is catalysed by Cr-doped sphene, but the catalytic effect decreases upon illumination. This electrocatalytic effect can be associated with the presence of Cr^V in such materials.

All these results illustrate the capabilities of the voltammetry of microparticles for providing chemical information on doped materials.

Experimental Section

Preparation and Characterisation of Specimens

We have used two methods of synthesis in order to show the industrial preparation of these ceramic pigmenting systems. The undoped and Cr-doped sphene were prepared by a sol-gel technique used previously.[5] The prepared samples contain an amount of chromium that replace the Sn cations, and in order to preserve the electroneutrality the divalent calcium cation was replaced by neodymium or ytrium trivalent cations. The prepared samples of the undoped $CaSnSiO_5$, $Ca_{0.95}Nd_{0.05}Sn_{0.95}Cr_{0.05}SiO_5$ and $Ca_{0.95}Y_{0.05}Sn_{0.95}Cr_{0.05}SiO_5$, are referred to as M-1, M-2 and M-3, respectively. An additional sample was prepared by replacing some of the silicium cations by aluminium cations, $Ca_{0.90}Y_{0.10}Sn_{0.95}Cr_{0.05}Si_{0.95}Al_{0.05}O_5$, and is referred to as M-4. Tetraethylorthosilicate (TEOS), $CaCl_2{\cdot}2H_2O$, $CrCl_3{\cdot}6H_2O$, and Y^{III} acetate (from Merck), $SnCl_2$ (from Aldrich) and $Nd(NO_3)_3{\cdot}6H_2O$ (from Rhône–Poulenc) were used as reagents. Gels were prepared by refluxing an ethanolic solution containing the required amounts of cation salts and TEOS at 70 °C. The TEOS/H_2O/ethanol molar ratio in the final solution was 1:12:20. The obtained gel was further dried at 120 °C.

The Cr-doped SnO_2 samples were prepared by a wet method that is similar to that described previously.[2] Samples with stoichiometry $Cr_xSn_{1-x}O_2$ (x = 0.05 and 0.1, referred to as M-5 and M-6) were prepared from $Cr(NO_3)_3{\cdot}6H_2O$ and SnO_2 (from Merck). First, the required amount of chromium nitrate was dissolved in distilled water. SnO_2 was then added to the above, and the final concentration of the solution was 0.05 mol·dm^{-3}. The obtained dispersion was heated whilst stirring until the water was removed. Further drying of the powdered sample was performed at 120 °C. Dried gels were thermally treated at several temperatures from 800 to 1300 °C with 2 h holding time.

H_2SO_4, $HClO_4$ (Panreac) and $NaClO_4$ (Merck) were used for electrolyte preparation. SnO_2 (Fluka) and Cr_2O_3 (Fluka) were used as reference materials. Electrocatalytic experiments were performed in solutions of $K_4Fe(CN)_6$ (Carlo Erba) and 1,4-dihydrobenzoquinone (Fluka).

Characterisation Techniques

The structural and microstructural features of the final pigmenting systems were examined using different techniques. X-ray diffraction analysis (Model D-500, Siemens, Karlsruhe, Germany) was performed using a graphite-monochromated Cu-K_a radiation. The diffractometer had two 1° divergence slits, the scatter and receiving slits were 1° and 0.05°, respectively.

UV/Vis spectra of the specimens (Model Lambda 9, Perkin–Elmer, Norwalk, Connecticut, U.S.A.) were obtained using the diffuse reflectance technique in the range of 200 to 1000 nm using a $BaSO_4$ plate as the reflectance standard. The absorbance was represented by the emission function, $F(R) = (1 - R)^2/2R$, where R is reflectance.

The microstructure of the final powdered samples was observed by field emission scanning electron microscopy at 30 kV (Model S-4100, Hitachi Ltd., Tokyo, Japan). To check the quality of the observation, some of the samples were etched with a diluted HF solution for 10 s and subsequently washed with distilled water.

Modified Electrode Preparation and Electrochemical Techniques

Paraffin-impregnated graphite electrodes (PIGEs) consist of cylindrical rods of graphite, with a diameter of 5 mm, which are impregnated under vacuum by paraffin. Preparation details are described in ref.[1]

To prepare sample-modified PIGEs, 0.1–1 mg of the material was powdered in an agate mortar and pestle, and placed on a glazed porcelain tile to form a spot of finely distributed material and then abrasively transferred to the surface of a PIGE by rubbing the electrode over that spot of sample.

Electrochemical experiments were performed at 298 K in a three-electrode cell under argon using a AgCl (3 M NaCl)/Ag reference electrode and a platinum-wire auxiliary electrode. Linear potential scan, cyclic and square wave voltammograms were obtained with BAS CV 50 W and CH I420 instruments. Unless stated, SQWVs were recorded by initiating the potential scan either at +0.85 and –0.85 V using a potential step increment of 4 mV and varying the square wave amplitude between 20 and 200 mV and the frequency between 2 and 200 Hz. Eventually semi-derivative convolution of data was performed in order to increase peak resolution.

Electrocatalytic experiments were performed in $K_4Fe(CN)_6$ solutions in two ways: (a) under dark conditions, confining the cell within the BAS CE-2 box, and (b) upon exposing the cell to direct illumination with conventional VIS and IR lamps located in azimuthal positions with respect to the electrochemical cell.

Supporting Information: (see footnote on the first page of this article). X-ray diffraction patterns of specimens thermally treated at final temperatures for 2 h: M1 at 1400 °C and M-5 and M-6 at 1300 °C; and field emission scanning electron microscopy micrographs of specimens thermally heated at 1300 °C.

[1] D. V. Shangani, G. R. Abrams, P. J. Smith, *Trans. J. Br. Ceram. Soc.* **1981**, *80*, 210–214.
[2] P. Escribano, C. Guillem, J. Alarcón, *Am. Ceram. Soc. Bull.* **1984**, *63*, 1492–1494.
[3] I. Ou-benmmou, H. Ahamdane, M. A. El idrisi, F. Bensamka, A. Mosset, M. L. El Idrisi, J. C. Jumas, *J. Eur. Ceram. Soc.* **2000**, *20*, 2159–2163.
[4] M. Muthuraman, K. C. Patil, *Mater. Res. Bull.* **1998**, *33*, 655–661.
[5] L. Ferrer, M. Sales, J. Alarcón, *Third Euro-Ceramics* **1993**, *2*, 935–938.
[6] E. Lopez-Navarrete, M. Ocaña, *J. Eur. Ceram. Soc.* **2002**, *22*, 353–359.
[7] E. Lopez-Navarrete, A. R. González-Elipe, M. Ocaña, *Ceram. Int.* **2003**, *29*, 385–392.
[8] F. Ren, S. Ishida, N. Takeuchi, K. Fujiyoshi, *Am. Ceram. Soc. Bull.* **1992**, *71*, 759–764.
[9] E. López-Navarrete, A. Caballero, V. M. Orera, F. J. Lázaro, M. Ocaña, *Acta Materialia* **2003**, *51*, 2371–2381.
[10] R. S. Pavlov, V. B. Marzá, J. B. Carda, *J. Mater. Chem.* **2002**, *12*, 2825–2832.
[11] B. Julián, H. Beltrán, E. Cordoncillo, P. Escribano, J. V. Folgado, V. Vallet-Regí, R. P. Del Real, *Eur. J. Inorg. Chem.* **2000**, *10*, 2694–2700.
[12] P. Maireles-Torres, P. Oliveira-Pastor, E. Rodríguez-Castellón, A. Jiménez-López, A. A. G. Tomlinson, *J. Solid State Chem.* **1991**, *94*, 368–380.
[13] V. Felice, B. Dussardier, J. K. Jones, G. Monnom, D. B. Ostrowsky, *Optical Mater.* **2001**, *16*, 269–277.
[14] F. Scholz, B. Meyer, *Electroanalytical Chemistry, A Series of Advances* (Eds.: A. J. Bard, I. Rubinstein), Marcel Dekker, New York, **1998**, *20*, p. 1.
[15] T. Grygar, F. Marken, U. Schröder, F. Scholz, *Collect. Czech. Chem. Commun.* **2002**, *67*, 163–208.
[16] H. A. Laitinen, *Denki Kagaku* **1976**, *44*, 626–631.
[17] S. Zhang, B. Meyer, G. Moh, F. Scholz, *Electroanalysis* **1995**, *7*, 319–328.
[18] A. Doménech, M. T. Doménech, M. T. *Electroanalysis*, in press.
[19] J. Liu, Z. H. Wang, Y. M. Wang, G. A. Luo, H. W. Sun, *Chinese Chem. Lett.* **2002**, *13*, 765–768.
[20] W. Y. Wang, C. M. Wang, *J. Chin. Chem. Soc.* **2000**, *47*, 405–414.
[21] D. Liu, P. V. Kamat, *J. Electrochem. Soc.* **1995**, *142*, 835–839.
[22] M. A. Blesa, P. J. Morando, A. E. Regazzoni, *Chemical dissolution of metal oxides.* CRC Press, Boca Raton, **1994**.
[23] L. G. Rodenas, P. J. Morando, M. A. Blesa, S. Duhalde, C. Saragovi, *Can. J. Chem.* **1993**, *71*, 771–778.
[24] L. G. Rodenas, M. Chocrón, P. J. Morando, M. A. Blesa, *Can. J. Chem.* **1996**, *74*, 103–106.
[25] T. Grygar, *J. Electroanal. Chem.* **1996**, *405*, 117–125.
[26] T. Grygar, *J. Solid State Electrochem.* **1998**, *2*, 127–136.
[27] T. Grygar, P. Bezdicka, *J. Solid State Electrochem.* **1998**, *3*, 31–38.
[28] A. Dostal, U. Schröder, F. Scholz, *Inorg. Chem.* **1995**, *34*, 1711–1717.
[29] A. M. Bond, R. Colton, F. Daniels, D. R. Fernando, F. Marken, Y. Nagaosa, R. F. M. Van Steveninck, J. N. Walter, *J. Am. Chem. Soc.* **1993**, *115*, 9556–9562.
[30] M. J. Carmezim, A. M. Simoes, M. O. Figueiredo, M. Da Cunha Belo, *Corros. Sci.* **2002**, *44*, 451–465.
[31] G. Horanyi, *J. Electroanal. Chem.* **1991**, *306*, 287–290.
[32] R. Bardykina, A. I. Falicheva, *Elektrokhimiya* **1987**, *23*, 1080–1086.
[33] J. M. Eckert, R. J. Judd, P. A. Lay, *Inorg. Chem.* **1987**, *26*, 2189–2191.
[34] M. Lovric, in *Electroanalytical Methods* (Ed.: F. Scholz), Springer, Berlin, **2002**, p. 111.
[35] A. Doménech, J. Alarcón, *J. Solid State Electrochem.* **2002**, *6*, 443–450.
[36] A. Doménech, F. J. Torres, J. Alarcón, *Electrochim. Acta* **2004**, *49*, 4623–4632.
[37] A. Doménech, F. J. Torres, J. Alarcón, *J. Solid State Electrochem.* **2004**, *8*, 127–137.
[38] A. M. Heyns, P. M. Harden, *J. Phys. Chem. Solids* **1999**, *60*, 277–284.
[39] A. Belletti, R. Borromei, L. Oleari, *Inorg. Chim. Acta* **1995**, *235*, 349–355.
[40] M. Lovric, F. Scholz, *J. Solid State Electrochem.* **1997**, *1*, 108–113.
[41] M. Lovric, F. Scholz, *J. Solid State Electrochem.* **1999**, *3*, 172–175.
[42] K. B. Oldham, *J. Solid State Electrochem.* **1998**, *2*, 367–377.
[43] U. Schröder, K. B. Oldham, J. C. Myland, P. J. Mahon, F. Scholz, *J. Solid State Electrochem.* **2000**, *4*, 314–324.
[44] A. M. Bond, F. Marken, *J. Electroanal. Chem.* **1994**, *372*, 125–135.
[45] A. M. Bond, J. B. Cooper, F. Marken, D. M. Way, *J. Electroanal. Chem.* **1995**, *396*, 407–418.
[46] S. Komorsky-Lovric, *J. Solid State Electrochem.* **1997**, *1*, 94–99.
[47] F. P. Koffyberg, F. A. Benko, *J. Appl. Phys.* **1982**, *53*, 1173–1177.
[48] P. Moretti, F. M. Michel-Calendini, *Phys. Rev. B* **1987**, *36*, 3522–3527.
[49] N. Sakai, Y. Ebina, K. Takada, T. Sasaki, *J. Am. Chem. Soc.* **2004**, *126*, 5851–5858.
[50] X. Long, Z. Lin, Z. Hu, G. Wang, *Chem. Phys. Lett.* **2004**, *392*, 192–195.
[51] G. A. Torchia, O. Martínez-Matos, P. Vaveliuk, J. O. Tocho, *Solid State Commun.* **2003**, *127*, 535–539.
[52] S. Kammoun, *J. Lumin.* **2004**, *106*, 205–210.
[53] M. Herren, H. Nishiuchi, M. Morita, *J. Chem. Phys.* **1994**, *101*, 4461–4462.

[54] S. Trasatti, *Pure Appl. Chem.* **1986**, *58*, 955–966.
[55] T. Kida, G. Guan, Y. Minami, T. Ma, A. Yoshida, *J. Mater. Chem.* **2003**, *13*, 1186–1191.
[56] Z.-K. Chen, W. Huang, L.-H. Wang, E.-T. Kang, B. J. Chen, C. S. Lee, S. T. Lee, *Macromolecules* **2000**, *33*, 9015–9025.
[57] M. S. Liu, X. Jiang, S. Liu, P. Herguth, A. K.-Y. Jen, *Macromolecules* **2002**, *35*, 3532–3538.
[58] C. P. Andrieux, J. M. Dumas-Bouchiat, J. M. Savéant, *J. Electroanal. Chem.* **1982**, *131*, 1–35.
[59] D. Garreau, P. Hapiot, J. M. Savéant, *J. Electroanal. Chem.* **1990**, *281*, 73–83.
[60] D. H. Evans, *Chem. Rev.* **1990**, *90*, 739–751.
Received: September 1, 2005
Published Online: December 13, 2005

